Effect of Liquid/Vapour Maldistribution on the Performance of Plate Heat Exchanger Evaporators

Jensen, Jonas Kjær; Kærn, Martin Ryhl; Ommen, Torben Schmidt; Markussen, Wiebke Brix; Reinholdt, Lars; Elmegaard, Brian

Published in:
Proceedings of the 24th IIR International Congress of Refrigeration

Publication date:
2015

Document Version
Peer reviewed version

EFFECT OF LIQUID/VAPOUR MALDISTRIBUTION ON THE PERFORMANCE OF PLATE HEAT EXCHANGER EVAPORATORS

Jonas K. JENSEN[(*)], Martin R. KÆRN[(*)], Torben OMMEN[(*)], Wiebke B. MARKUSSEN[(*)], Lars REINHOLDT[(**)], Brian ELMEGAARD[(*)]

[(*)] Department of Mechanical Engineering, Technical University of Denmark, Nils Koppels Allé Building 403, Kgs. Lyngby, DK-2800, Denmark

jkjje@mek.dtu.dk

[(**)] Danish Technological Institute, Kongsvang Allé 29, Aarhus, DK-8000, Denmark

ABSTRACT

Plate heat exchangers are often applied as evaporators in industrial refrigeration and heat pump systems. In the design and modelling of such heat exchangers the flow and liquid/vapour distribution is often assumed to be ideal. However, maldistribution may occur and will cause each channel to behave differently due to the variation of the mass flux and vapour quality. To evaluate the effect of maldistribution on the performance of plate heat exchangers, a numerical model is developed in which the mass, momentum and energy balances are applied individually to each channel, including suitable correlations for heat transfer and pressure drop. The flow distribution on both the refrigerant and secondary side is determined based on equal pressure drop while the liquid/vapour distribution is imposed to the model. Results show that maldistribution may cause up to a 25 % reduction of the overall heat transfer coefficient, compared to a lumped model with uniform distribution.

1. INTRODUCTION

Plate heat exchangers (PHE) are often applied as evaporators for industrial scale refrigeration or heat pump systems. The performance of such heat exchangers is thus important for the design and evaluation of these systems. Often, when dimensioning such heat exchangers, a lumped model with uniform flow and vapour quality distribution is applied. Thus, the effect of the end-plates is neglected. Maldistribution may occur and pose an impact on the heat transfer performance (Mueller and Chiou, 1988).

Kandlikar and Shah (1989) provides correction factors for the logarithmic mean temperature difference, for several types of PHE configurations, to account for the end-plate effects. However, these are applicable only for liquid/liquid heat transfer without flow maldistribution. Bassiouny and Martin (1983) investigated the flow distribution in PHE and found that flow maldistribution can be avoided if the area ratio between the inlet port and outlet port is chosen correctly. However, again for liquid/liquid heat transfer only.

The effect of maldistribution in evaporators was investigated for mini-channel heat exchangers in Brix et al. (2009) and Brix et al. (2010) and for fin and tube evaporators in Kærn et al. (2011). These studies were focused on quantifying the effect of a non-uniform airflow distribution and found that the refrigerant distribution was affected by the airflow distribution and that the distribution has an effect on the evaporator performance.

Lin et al. (2014) experimentally investigated the in-channel distribution of refrigerant and its effect on the heat transfer characteristics of PHE. Vist and Pettersen (2004) experimentally investigated the quality distribution in compact heat exchanger manifolds and showed that the liquid/vapour maldistribution can be severe and cause a significant reduction of the thermal performance of the heat exchanger.

In the present study, a numerical model of a PHE capable of solving heat transfer, pressure loss and mass flow distribution will be presented. In this model the vapour quality distribution (the vapour quality at the inlet of the refrigerant channels) is imposed. Thus the effect of the vapour quality distribution and the induced mass flow maldistribution can be quantified.

2. METHOD

2.1. Plate heat exchanger correlations, maldistribution parameter and operating conditions

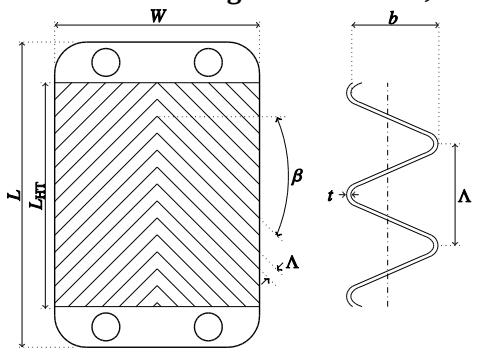

Figure 1. Schematic diagram of a chevron corrugated plate.

Table 1. Plate dimensions of plate 1 & 2

	Plate 1	Plate 2
W	115 mm	243 mm
L	522 mm	525 mm
L_{HT}	476 mm	456 mm
β	35 °	35 °
Λ	8 mm	8 mm
t	0.5 mm	0.5 mm
b	2.3 mm	2.3 mm
λ	16 W/m-K	16 W/m-K
D_h	$2(b-t)\,\phi^{-1}$	

The numerical model was developed in MatLAB (2013) using the thermophysical property database CoolProp (Bell et al., 2014). Correlations proposed by Han et al. (2003) were applied for calculating heat transfer and pressure drop in the two-phase region, while Martin (1996) was applied for the single-phase regions of both the refrigerant and the secondary sides.

The refrigerant was R134a and the secondary side was assumed to be water. Two plate dimensions were investigated: Plate 1 and Plate 2. The dimensions of these two plates are stated in Table 1. As seen Plate 1 has a smaller length to width ratio than Plate 2. The PHE had 20 refrigerant channels.

In order to best isolate the effect of the vapour quality distribution, fixed operating conditions were applied. The applied operating conditions for the secondary side consisted of a fixed inlet and outlet temperature: $T_{\mathrm{sec,in}}$=40 °C and $T_{\mathrm{sec,out}}$=30 °C. For the refrigerant, a fixed superheat temperature difference: ΔT_{SH}=5 K and a constant inlet specific enthalpy were applied. The inlet specific enthalpy was evaluated at saturated liquid conditions at 60 °C.

The vapour quality distribution was imposed by the parameter Δx, which is the difference between the inlet vapour quality of the first and last refrigerant channel. The vapour quality distribution profile was assumed to be linear and thus the inlet quality, $x_{\mathrm{in},n}$, of the remaining channels was found as shown in Eq. (1). Here N is the total number of refrigerant channels and n is the index of the refrigerant channels. The value of $x_{\mathrm{in},1}$ is solved iteratively to ensure mass conservation. This will be described in detail in section 2.2.

$$x_{\mathrm{in},n} = x_{\mathrm{in},1} - (1-n)\frac{\Delta x}{N-1} \qquad \text{for } n \in \{1, \mathrm{N}\} \tag{1}$$

2.2. Solving heat transfer and pressure loss

The heat transfer and pressure loss was solved for given boundary conditions (refrigerant and secondary side inlet conditions) using a successive substitution approach. The control volume and grid structure are illustrated in Figure 2. As seen the PHE is constructed such that both the first and the last channels are secondary channels and thus: $M=N+1$, where N and M are the number of refrigerant and secondary channels, respectively. Further, the total number of plates, I, can be determined as $I=2N+2$ in which two of the plates are end plates and therefore do not transfer heat: $\dot{Q}_{1,j} = \dot{Q}_{I,j} = 0$. Thus the number heat transfer plates are $I=2N$. A total of J=100 lengthwise discretizations were applied.

The structure of the successive substitution procedure is seen in Figure 3 (A). As seen first initial guess values were supplied for: $\dot{Q}_{i,j}, T_{w,\mathrm{sec},i,j}, T_{w,\mathrm{ref},i,j}, \Delta p_{ref,i,j}$ and $\Delta p_{\mathrm{sec},i,j}$. From $\Delta p_{ref,i,j}$ and $\Delta p_{\mathrm{sec},i,j}$ the pressure of the remaining cells was found as seen in Eq. (2)-(3). From $\dot{Q}_{i,j}$ the enthalpy of all cells was found from the energy balances: Eq. (4)-(5)

$$p_{\mathrm{ref},n,j+1} = p_{\mathrm{ref},n,j} + \Delta p_{\mathrm{ref},n,j} \quad \text{for } n \in \{1,N\} \quad \text{and } j \in \{1,\mathrm{J}\} \quad (2)$$

$$p_{\mathrm{sec},m,j+1} = p_{\mathrm{sec},m,j} - \Delta p_{\mathrm{sec},m,j} \quad \text{for } m \in \{1,M\} \quad \text{and } j \in \{1,\mathrm{J}\} \quad (3)$$

$$h_{ref,n,j+1} = h_{ref,n,j} + \frac{\dot{Q}_{2\cdot n,j} + \dot{Q}_{2\cdot n+1,j}}{\dot{m}_{\mathrm{ref},n}} \quad \text{for } n \in \{1,N\} \quad \text{and } j \in \{1,\mathrm{J}\} \quad (4)$$

$$h_{sec,m,j+1} = h_{sec,m,j} - \frac{\dot{Q}_{2\cdot m-1,j} + \dot{Q}_{2\cdot m,j}}{\dot{m}_{\mathrm{sec},m}} \quad \text{for } m \in \{1,M\} \quad \text{and } j \in \{1,\mathrm{J}\} \quad (5)$$

From the pressure and enthalpy, the temperatures at the inlet and outlet of all cells were determined and subsequently the log mean temperature difference, $\Delta T_{\mathrm{LM},i,j}$ between each control volume was found as seen in Eq. (6). Here $p(i)$= {1, 1, 2, 2, 3, 3, … M, M} and $q(i)$= {-, 1, 1, 2, 2, 3, 3, ... N, N,-} for $i \in \{1,\mathrm{I}\}$ which ensures that the correct channel is chosen for each plate.

$$\Delta T_{LM,i,j} = \frac{\left(T_{\mathrm{sec},p(i),j} - T_{ref,q(i),j}\right) - \left(T_{\mathrm{sec},p(i),j+1} - T_{ref,q(i),j+1}\right)}{ln\left(\frac{T_{\mathrm{sec},p(i),j} - T_{ref,q(i),j}}{T_{\mathrm{sec},p(i),j+1} - T_{ref,q(i),j+1}}\right)} \quad \text{for } i \in \{2,\mathrm{I}-1\} \quad \text{and } j \in \{1,\mathrm{J}\} \quad (6)$$

The heat transfer coefficient and friction factor were determined from the applied correlations. Transport properties were evaluated at the cells mean temperature and pressure. From the heat transfer coefficients of the cell walls the overall heat transfer coefficient between each control volume was determined from Eq. (7).

$$U_{i,j} = \left(\frac{1}{\alpha_{\mathrm{sec},i,j}} + \frac{t}{\lambda} + \frac{1}{\alpha_{\mathrm{ref},i,j}}\right)^{-1} \quad \text{for } i \in \{2,\mathrm{I}-1\} \quad \text{and } j \in \{1,\mathrm{J}\} \quad (7)$$

Subsequently $\dot{Q}_{i,j}, T_{w,\mathrm{sec},i,j}, T_{w,\mathrm{ref},i,j}, \Delta p_{ref,n,j}$ and $\Delta p_{\mathrm{sec},m,j}$ was updated based on the calculated temperature difference, heat transfer coefficient and friction factor. This was done as seen in Eq. (8)-(12). For the cell pressure loss an average of the friction factors of the cell's two opposing plates were applied as: $\bar{\xi}_{\mathrm{ref},n,j} = 0.5 \cdot \left(\xi_{\mathrm{ref},2\cdot n,j} + \xi_{\mathrm{ref},2\cdot n+1,j}\right)$ and $\bar{\xi}_{\mathrm{sec},n,j} = 0.5 \cdot \left(\xi_{\mathrm{sec},2\cdot m,j} + \xi_{\mathrm{sec},2\cdot m+1,j}\right)$.

$$\dot{Q}_{i,j} = q''_{i,j} A_{i,j} = U_{i,j} \cdot A_{i,j} \cdot \Delta T_{LM,i,j} \quad \text{for } i \in \{2,\mathrm{I}-1\} \quad \text{and } j \in \{1,\mathrm{J}\} \quad (8)$$

$$T_{w,\mathrm{sec},i,j} = 0.5 \cdot \left(T_{\mathrm{sec},m,j} + T_{\mathrm{sec},m,j+1}\right) - q''_{i,j} \frac{1}{\alpha_{\mathrm{sec},i,j}} \quad \text{for } i \in \{1,\mathrm{I}\} \quad \text{and } j \in \{1,\mathrm{J}\} \quad (9)$$

$$T_{w,\mathrm{ref},i,j} = T_{w,\mathrm{sec},i,j} - q''_{i,j} \frac{t}{\lambda} \quad \text{for } i \in \{2,\mathrm{I}-1\} \quad \text{and } j \in \{1,\mathrm{J}\} \quad (10)$$

$$\Delta p_{\mathrm{ref},n,j} = \frac{2 \cdot G_{\mathrm{ref},n}^2 \cdot \bar{\xi}_{\mathrm{ref},n,j} \cdot \frac{L_{HT}}{J}}{\rho_{\mathrm{ref},n,j} \cdot D_h}, \quad \text{for } n \in \{1,N\} \quad \text{and } j \in \{1,\mathrm{J}\} \quad (11)$$

$$\Delta p_{\mathrm{sec},m,j} = \frac{2 \cdot G_{\mathrm{sec},m}^2 \cdot \bar{\xi}_{\mathrm{sec},n,j} \cdot \frac{L_{HT}}{J}}{\rho_{\mathrm{sec},m,j} \cdot D_h} \quad \text{for } m \in \{1,M\} \quad \text{and } j \in \{1,\mathrm{J}\} \quad (12)$$

To determine if a solution was reached, the relative difference between the guess values and the updated values of: $\dot{Q}_{i,j}, T_{w,\mathrm{sec},i,j}, T_{w,\mathrm{ref},i,j}, \Delta p_{ref,i,j}$ and $\Delta p_{\mathrm{sec},i,j}$ was calculated. If the maximum relative difference was below the desired tolerance the procedure was terminated. If it was greater than the desired tolerance: the updated values were supplied as guess values for the next iteration.

2.3. Solving flow distribution and operating conditions

To solve the flow distribution and the operating conditions a Newton-Raphson solver was applied. The structure of the procedure is seen in Figure 3 (B). The flow distribution was solved for both refrigerant and secondary side such that equal pressure loss over each channel was attained. The objective was to find a mass flow rate for each channel such that this criterion was satisfied. The pressure loss in each channel was found using the successive substitution approach described above. The flow distribution was calculated to satisfy Eq. (13) – (14). The first *N*-1 and *M*-1 equations ensure that equal pressure loss is attained, while equations *N* and *M* ensure mass conservation.

$$\sum_{j=1}^{J} \Delta p_{\mathrm{ref},n,j} = \frac{1}{N} \sum_{n=1}^{N} \sum_{j=1}^{J} \Delta p_{\mathrm{ref},n,j} \qquad \text{for } n \in \{1, N-1\} \qquad \dot{m}_{\mathrm{ref,tot}} = \sum_{n=1}^{N} \dot{m}_{\mathrm{ref},n} \tag{13}$$

$$\sum_{j=1}^{J} \Delta p_{\mathrm{sec},m,j} = \frac{1}{M} \sum_{m=1}^{M} \sum_{j=1}^{J} \Delta p_{\mathrm{sec},m,j} \qquad \text{for } m \in \{1, M-1\} \qquad \dot{m}_{\mathrm{sec,tot}} = \sum_{m=1}^{M} \dot{m}_{\mathrm{sec},m} \tag{14}$$

To solve the fixed operating conditions described in Section 2.1 equations Eq. (15)-(17) were applied. Here Eq. (15) was used to determine the needed refrigerant mass flow rate, $\dot{m}_{\mathrm{ref,tot}}$, in order to ensure that the desired superheat was attained at the outlet of the PHE. The superheat was defined using enthalpies thus avoiding the zero singularity at ΔT_{SH}=0 K (two-phase refrigerant outlet). $h_{\Delta T_{SH}}$ was evaluated at the outlet pressure and a temperature ΔT_{SH} above the corresponding saturation temperature. Eq. (16) was applied to determine the evaporation temperature needed to ensure the desired secondary outlet temperature. $h_{T_{\mathrm{sec},o}}$ was evaluated at the desired secondary outlet temperature and the calculated pressure. Finally, Eq. (17) was applied to determine the inlet vapour quality of the first channel to ensure conservation of the inflowing vapour.

$$h_{\Delta T_{SH}} = \frac{1}{\dot{m}_{\mathrm{ref,tot}}} \sum_{n=1}^{N} \dot{m}_{\mathrm{ref},n} \cdot \mathrm{h}_{\mathrm{ref},n} \tag{15}$$

$$h_{T_{\mathrm{sec},o}} = \frac{1}{\dot{m}_{\mathrm{sec,tot}}} \sum_{m=1}^{M} \dot{m}_{\mathrm{sec},n} \cdot \mathrm{h}_{\mathrm{sec},n} \tag{16}$$

$$\mathrm{x}_{\mathrm{ref,in}} \cdot \dot{m}_{\mathrm{ref,tot}} = \sum_{n=1}^{N} \dot{m}_{\mathrm{ref},n}\, x_{\mathrm{ref,in},n} \tag{17}$$

The flow distribution and operating conditions were solved to a relative tolerance one order of magnitude higher than that applied in the successive substitution procedure, which had a tolerance of 10^{-5}.

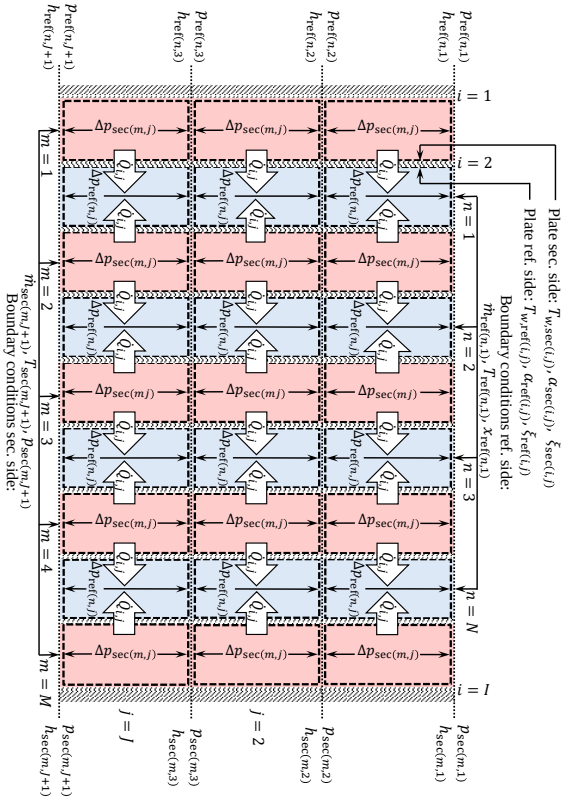

Figure 3. Control volume and grid structure diagram

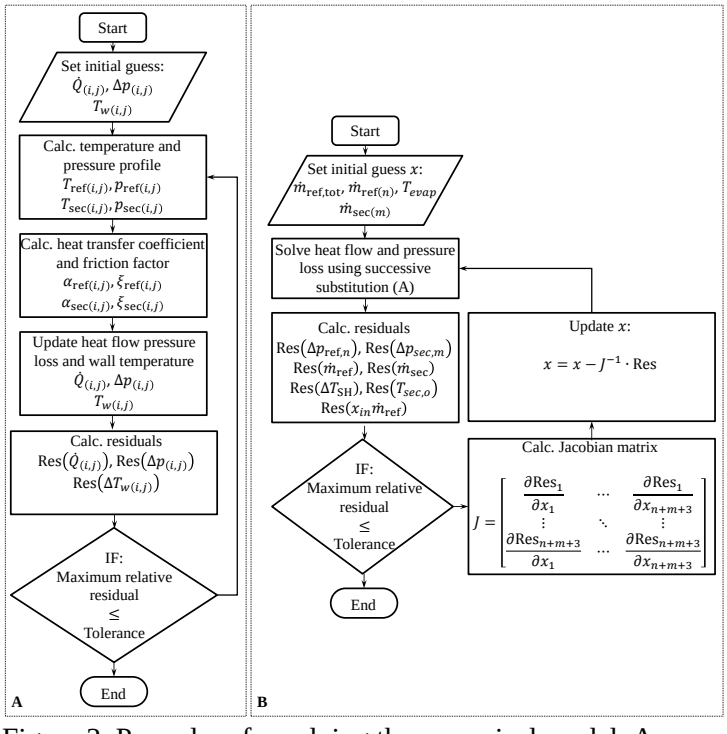

Figure 2. Procedure for solving the numerical model. A: solves the heat transfer and pressure drop. B: solves flow distribution and operating conditions.

3. RESULTS

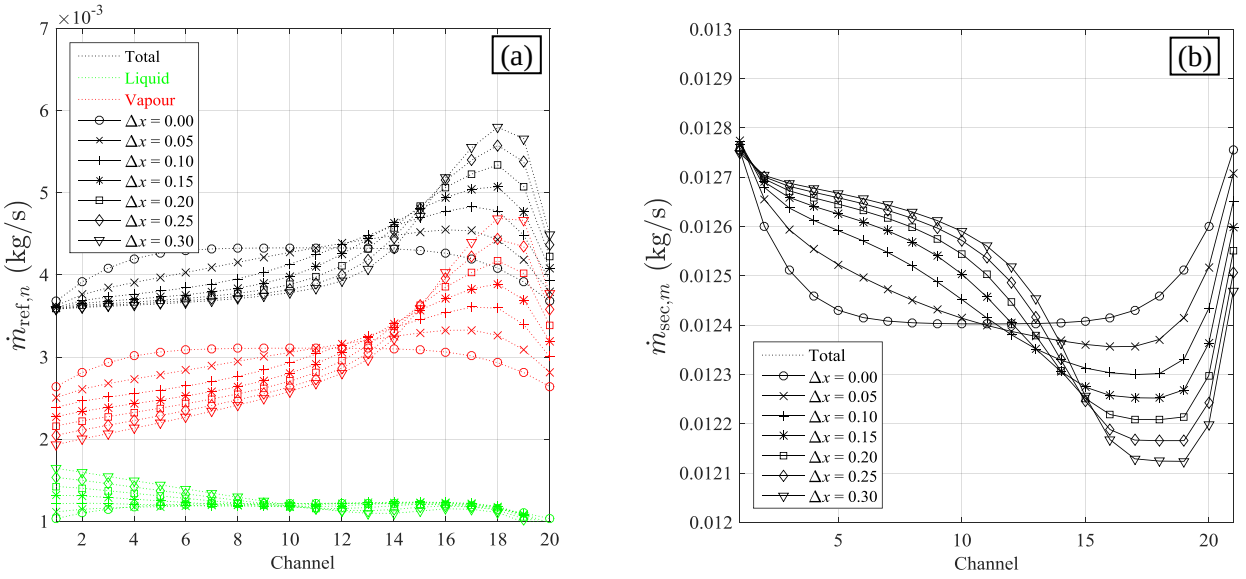

Figure 4. Refrigerant (a) and secondary (b) mass distribution profile for plate type 1 with a mean heat flux of 5000 W/m^2 and a variation of the vapour quality distribution.

In order to quantify the effect of a non-uniform distribution of vapour quality a series of simulations have been conducted. The simulations have been carried out for the two plate sizes listed in Table 1 under four different mean heat fluxes: 2500 W m^{-2}, 5000 W m^{-2}, 7500 W m^{-2}, 10,000 W m^{-2}, yielding a total of eight cases. For these eight cases the quality distribution was varied from a uniform distribution (Δx=0) to high maldistribution (Δx=0.4). All simulations were performed with N=20 refrigerant channels and the operating conditions described in Section 2.1.

An example of the mass distribution variation is shown in Figure 4 for a mean heat flux of 5000 W m^{-2} and plate size 1. As seen, even with a uniform distribution of the vapour quality (Δx=0) maldistribution of the mass flow rates will occur for both the refrigerant and the secondary side. This maldistribution is caused by the effects of the end plates and affects the mass flow rate of the first and last five channels for the presented case.

When increasing Δx, it is seen that the variation of the mass flow rates is increased such that more refrigerant mass flow is supplied to the channels with low vapour quality. Conversely, less secondary mass flow is supplied to the adjacent secondary channels. Overall it is seen from Figure 4 that the variation of the mass flow rate is more profound on the refrigerant side than on the secondary side.

Figure 5 shows the temperature and heat flux profile for two cases: uniform vapour quality distribution (Δx=0) and with vapour quality maldistribution of Δx=0.3. Figure 5 (a) & (b) shows the temperature of the refrigerant and secondary channels as well as the wall temperature on both sides. As seen from Figure 5 (a), a uniform temperature profile occurs in the centre of the heat exchangers when the vapour quality distribution is ideal. However, the first and last 5 channels will differ from this due to the effect of the end plates, which results in a low temperature difference at the refrigerant outlet side, consequently reducing the heat flux in this area, see Figure 5 (c).

Imposing a vapour quality maldistribution of Δx=0.3 results in a non-uniform temperature profile as seen in Figure 5 (b). As seen the high vapour quality of the 10 first channels result in a large region in which the refrigerant is superheated. This region will subsequently suffer from both low temperature differences and poor heat transfer coefficients. These unfavourable conditions are enhanced by the additionally low mass flux caused by the high pressure loss associated with the superheated vapour. Consequently, the heat flux in this region will be low as is evident from Figure 5 (d).

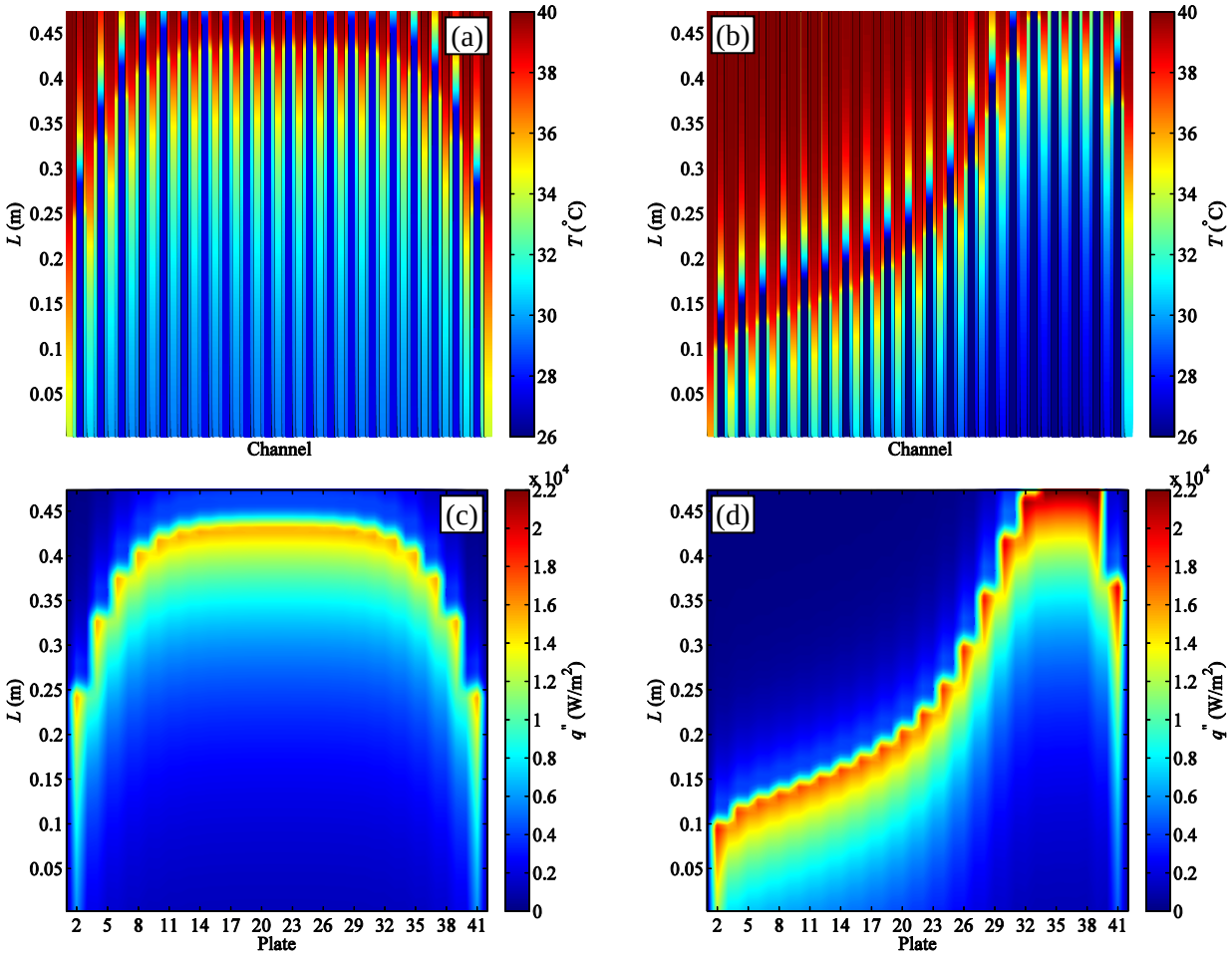

Figure 5 Temperature (a) & (b) and heat flux (c) & (d) profile for plate type 1 with a mean heat flux of 5000 W m^{-2}. Even vapour quality distribution (Δx=0) is presented in (a) & (c). Vapour quality maldistribution (Δx=0.30) is presented in (b) & (d).

Figure 6 summarizes the results of the eight simulated cases. Here the needed evaporation temperature, T_{evap}, the overall heat transfer coefficient reduction factor, F, and the relative standard deviation, RSD, for both the refrigerant and secondary mass flow distribution, is presented. These four parameters are all shown as functions of the imposed vapour quality distribution parameter Δx.

As seen from Figure 6 (a) the evaporation temperature only shows a weak dependence on the plate size while exhibiting a large dependence on both the mean heat flux and Δx. Further, it may be seen that the larger the heat flux, the more sensitive the evaporation temperature will be on the vapour quality distribution. Figure 6 (b) shows the reduction factor, F, of the overall heat transfer coefficient compared to a lumped model in which uniform vapour quality distribution is assumed and the effect of the end plates are neglected. As seen, even with Δx=0 there is a reduction of the overall heat transfer coefficients due to the end plates. This reduction depends on both the plate size and mean heat flux. As seen, when the heat flux is increased the heat transfer coefficient is more affected by the end plates. This is however caused by the increased mass flux associated with the increased heat flux as the plate geometry is fixed. Further, it may be seen that Plate 1 is more influenced by the end plates than Plate 2. This is attributed to the small length to width ratio for Plate 1: ≈ ¼ compared to the larger ratio of ≈ ½ for Plate 2. Thus the mass flux for will be higher for Plate 1 than for Plate 2. It is seen that the two plate sizes are equally influenced by Δx.

Figure 6 (c) & (d) show the relative standard deviation (RSD) of the mass distribution and is thus a measure of the variability of the mass flow profiles. Hence, if RSD=0 % the mass flow rates do not deviate from the mean and a uniform distribution is attained. As seen this is never the case. From Figure 6 (c) it is clear that the maldistribution induced by the end plates increases with increasing heat flux and that the maldistribution is influenced by the plate size. The refrigerant maldistribution increases with the mean heat flux while it is

seen that the secondary side maldistribution decreases. Furthermore, the refrigerant maldistribution is more influences by the plate size than the secondary side.

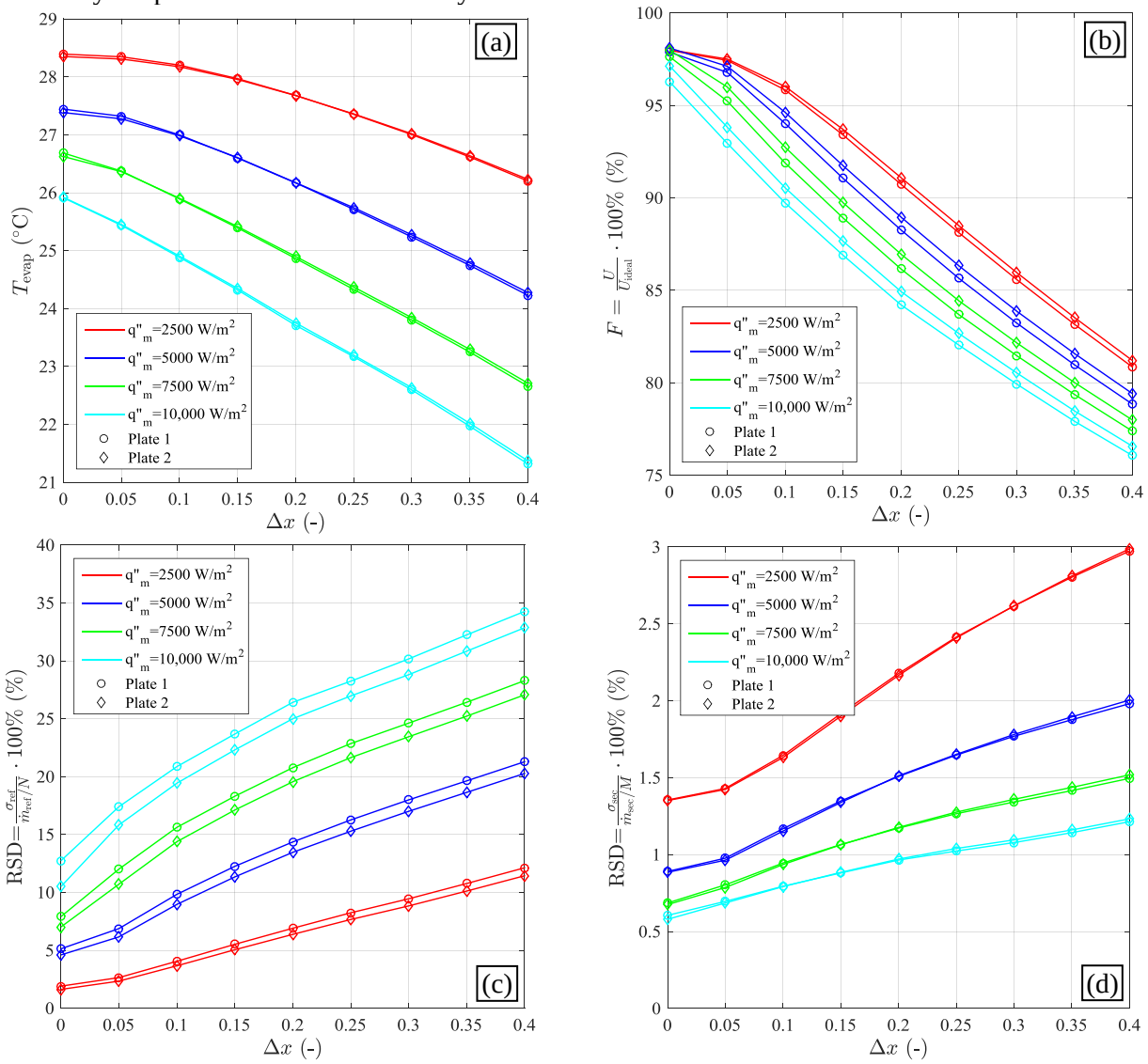

Figure 6. Evaporation temperature (a), the overall heat transfer coefficient reduction factor (b) and the relative standard deviation, RSD, for both the refrigerant (c) and secondary (d) mass flow distribution.

4. DISCUSSION

The results presented stem solely from numerical simulations using validated heat transfer and pressure loss correlations. However, it is unclear from the sources of the correlations to which extent they include some effect of maldistribution. Therefore, the absolute values of the local overall heat transfer coefficients attained by the described model may be inaccurate. However, the relative reduction of heat transfer coefficient and the RSD should be justified, as the same correlations are applied.

5. CONCLUSIONS

A numerical model of a plate evaporator was developed such that a vapour quality distribution profile could be imposed, thus allowing the influence of the distribution to be quantified. Eight cases were simulated: four mean heat fluxes and two plate sizes. This showed that vapour quality maldistribution can reduce the *U*-value up to 25% when the vapour quality distribution difference is 0.4. Further it was found that even with a uniform vapour quality distribution; flow maldistribution will occur and may cause a reduction of the *U*-value from 2-4%. This is caused by the end plates and the effect is increased with increasing mean heat flux. Further the plate with the smallest length to width ratio showed a stronger tendency for maldistribution.

6. REFERENCES

Bassiouny, M.K., Martin, H., 1983. Flow distribution and pressure drop in plate heat exchangers - I. Chem. Eng. Sci. 39, 693–700.

Bell, I.H., Wronski, J., Quoilin, S., Lemort, V., 2014. Pure and Pseudo-pure Fluid Thermophysical Property Evaluation and the Open-Source Thermophysical Property Library CoolProp. Ind. Eng. Chem. Res. 53, 2498–2508.

Brix, W., Kærn, M.R., Elmegaard, B., 2009. Modelling refrigerant distribution in microchannel evaporators. Int. J. Refrig. 32, 1736–1743.

Brix, W., Kærn, M.R., Elmegaard, B., 2010. Modelling distribution of evaporating CO2 in parallel minichannels. Int. J. Refrig. 33, 1086–1094.

Han, D.H., Lee, K.J., Kim, Y.H., 2003. Experiments on the characteristics of evaporation of R410A in brazed plate heat exchangers with different geometric configurations. Appl. Therm. Eng. 23, 1209–1225.

Kandlikar, S.G., Shah, R.K., 1989. Multipass plate heat exchangers - effectiveness-NTU results and guidelines for selecting pass arrangements. J. Heat Transfer 111, 300–313.

Kærn, M.R., Brix, W., Elmegaard, B., Larsen, L.F.S., 2011. Performance of residential air-conditioning systems with flow maldistribution in fin-and-tube evaporators. Int. J. Refrig. 34, 696–706.

Lin, Y.-H., Li, G.-C., Yang, C.-Y., 2014. An experimental observation of the effect of flow direction for evaporation heat transfer in plate heat exchanger. Appl. Therm. Eng. 1–8.

Martin, H., 1996. A theoretical approach to predict the performance of chevron-type plate heat exchangers. Chem. Eng. Process. 35, 301–310.

MatLAB, version: 2013b, publisher: Mathworks, 2013.

Mueller, A.C., Chiou, J.P., 1988. Review of various types of flow maldistribution in heat exchangers. Heat Transf. Eng. 9, 36–50.

Vist, S., Pettersen, J., 2004. Two-phase flow distribution in compact heat exchanger manifolds. Exp. Therm. Fluid Sci. 28, 209–215.

7. NOMENCLATURE

Symbols

A	Area	m^2
b	Plate press depth	m
D_h	Hydraulic diameter	m
F	Heat transfer reduction factor	%
G	Mass flux	kg s^{-1} m^{-2}
h	Specific enthalpy	kJ kg^{-1}
I	Number of plates	-
J	Number of discretization	-
L	Plate length	m
M	Number of secondary channels	-
$\dot{m}$	Mass flow rate	kg s^{-1}
N	Number of refrigerant channels	-
p	Pressure	Pa
$\dot{Q}$	Heat load	kW
q''	Heat flux	kW m^{-2}
RSD	Relative standard deviation	%
T	Temperature	°C
t	Plate thickness	m
U	Overall heat transfer coefficient	kW m^{-2} K^{-1}
W	Plate width	m
x	Vapour quality	-

Greek

α	Heat transfer coefficient	kW m^{-2} K^{-1}
β	Plate corrugation angle	°
Δ	Difference	-
λ	Thermal conductivity	kW m^{-1} K^{-1}
Λ	Plate corrugation spacing	m
μ	Viscosity	Pa s
ξ	Fanning friction factor	-
ρ	Density	kg m^{-3}
σ	Standard deviation	-
ϕ	Plate enhancement factor	-

Subscripts & indices

HT	Plate heat transfer section
i	Plate index
j	Discretization index
m	Secondary channel index
n	Refrigerant channel index
sec	Secondary
ref	Refrigerant
w	Wall